Vehicle System Dynamics
Vol. 00, No. 00, month 2008, 1–25

RESEARCH ARTICLE

The simulation of in-plane tyre modal behaviour: A broad modal range comparison between analytical and discretized modelling approaches

Achillefs Tsotras* and George Mavros

Aeronautical and Automotive Engineering Department, Loughborough University, Leicestershire, LE11 3TU, UK ;
(*Received 00 Month 200x; final version received 00 Month 200x*)

In-plane tyre modal behaviour determines the response of tyres to ride excitations and braking/traction manoeuvres. In many studies, the interest is limited to relatively low frequencies and a detailed investigation into the ability of models to accurately simulate higher order responses is unnecessary. In cases where an in-plane model is to be used for the generation of the contact deformation and stresses, or where modal reduction methods are implemented, a detailed knowledge of the modal response is desirable. The present work forms a study on the ability of a number of frequently used modelling approaches to generate realistic modal data throughout a wide frequency range. The analytical ring on elastic foundation model is used as a benchmark throughout the paper. Its predictions are compared with those of two discretized models, namely a truss-based and a beam-based model. The sensitivity of the ring's response to a number of physical parameters is discussed. The results are used to inform the comparison between the analytical ring and the discretized models, providing explanations for any discrepancies observed. The limited applicability of the truss model is pointed out, while the accuracy of the beam-based model is enhanced by a circumferential inextensible string element. Both the ring and the enhanced beam models are further improved with the addition of a non-linear string-based sidewall which accounts for the change in sidewall stiffness with inflation pressure. The findings may offer a reference when setting up in-plane models, including the stage of planning modal tests for parameter identification.

Keywords: in-plane tyre vibrations; modal tyre; ring tyre model; finite elements tyre model; tyre inflation effect; nonlinear tyre sidewall;

1. Introduction

Tyre performance is vital for the dynamic behaviour of a vehicle, as tyres represent the sole contact force generation interface between the vehicle and the road. The present work is part of a larger project aiming to investigate the influence on vehicle dynamics (in particular extreme traction manoeuvres) of the interaction between shear force generation and in-plane modal behaviour. It is recognized that under such conditions tyre shear forces change rapidly, possibly as a result of non-linear friction conditions. Such excitations directly affect the tyre belt but also excite secondary ride dynamics which in turn influence shear force generation in a closed loop manner.

Under these circumstances the interaction between vertical suspension motion and the radial response of the tyre belt is expected to play a significant role in the

*Corresponding author. Email: a.tsotras@lboro.ac.uk

ISSN: 0042-3114 print/ISSN 1744-5159 online

DOI: 10.1080/0042311YYxxxxxxxx
http://www.informaworld.com

vertical load distribution. Due to the accuracy required in order to obtain representative load distributions through modal response and also because relatively higher frequencies are involved in such phenomena, it is beneficial to investigate the ability of various modelling approaches in accurately depicting the modal behaviour of tyres, under typical contact-rotation operating conditions.

In this first part of the study, the well established ring on elastic foundation model is briefly presented in comparison to typical discretized modelling approaches, with respect to modal behaviour simulation. The non linear inflation pressure effect is also incorporated in the modal simulation of both analytical and discretized approaches, through both belt and sidewall stiffening behaviour. The total effect of inflation pretension is presented, with regards to modal data prediction.

The study is not limited to the low frequency range, typical of vehicle dynamics oriented tyre studies, as the demanded representation accuracy of contact deformation necessitates a frequency range much broader than the one typically examined in vehicle dynamics studies [1]. The aim is to identify the effect of different modelling techniques on a tyre model derived by a modal expansion and reduction process.

2. Tyre modelling approaches

The literature is rich in physical tyre models, as well as empirical, experimentally derived ones. A detailed presentation of both can be found in [2]. Within the family of existing physical models, two main trends can be identified with regards to the incorporation of the vibrational response of the tyre structure to road inputs:

- **Tyre vibration (modal) models**. They focus on the tyre response to road surface profile irregularities, or to the harmonic excitation induced by the rolling contact. Usually, tyre response is examined from an NVH point of view. At the lower frequency range, the primary concern is vibration transmissivity to the rest of the vehicle, through the wheel and suspension. At higher frequencies, noise generation becomes the main focus of investigation. Modelling of the whole tyre structure and shape is essential for an accurate modal behaviour representation. In most such studies, the actual contact deformation and the way it influences shear force generation is not investigated.
- **Tyre shear force generation models**. They focus on the interaction between the road and the tyre, aiming to accurately predict the shear forces at the contact, as an input to vehicle dynamics simulation models. Tyre contact deformation is examined, as it directly affects the generation of friction forces.

2.1. *Simulation of tyre modal behaviour*

Tyre vibration models aim to accurately predict tyre natural frequencies and deformation mode shapes. Due to their focus on the structural response, the tyre/road interaction is modelled in a simplified manner, either as an a priori induced single point excitation, or as a time-invariant boundary condition based on a finite contact length assumption. Their transient-vibrational character is owed to their ability to simulate the response to transient (harmonic or not) excitations, albeit assuming simplified,steady, boundary conditions [3, 4].

The analytical ring on elastic foundation under inflation pretension offers a valuable and experimentally verified 2-dimensional modal simulation tool, at least up to a certain frequency value. The ring model, introduced in [5, 6], offers great computational effectiveness, through the expression of its response using the su-

perposition of its modes. Starting from a known modal behaviour of a non rotating and non contacting tyre, Soedel and Prasad [7] calculated the modal behaviour under point contact conditions. Rotation was later added to the analytical modal calculation by Huang, as presented in a series of articles[8–11]. Moving from the point contact assumption towards a more realistic contact representation, Zegelaar in [3] combined the analytical ring solution with a vertical Winkler bedding [12] in order to acquire modal behaviour under certain contact conditions. A modally expanded ring model is also used in [13], in combination with a spectral density description of the road roughness, in a noise generation study.

Tyre modal simulation is generally associated with frequency domain studies, in which the response to a harmonic excitation within a certain frequency range is sought. An excitation of harmonic nature, though, cannot be assumed in the general case of the rolling frictional contact, because of the strong non-linear character of the generated shear forces. A time domain solution must be sought in this case, as underlined in [14], where a solution is acquired through a number of convolution integrals.

In studies based on the analytical ring model, modal expansion is the preferable method to acquire the structural response, since a space discretization, as the one presented in [15], is computationally more demanding. Modal expansion is also a computationally efficient method for acquiring the response of discretized finite element models. A time-based solution may be calculated with the use of a modally expanded finite element model as presented in [4].

One could argue that a modelling approach based on modal expansion of a tyre operating under certain contact/rotation conditions is rather restrictive, as modal expansion is performed under constant boundary conditions. In contrast, transient tyre operation may result in varying boundary conditions, and, especially under abrupt handling manoeuvres, the sidewall could manifest a severely non-linear response. Hence it becomes clear that the actual size of the contact area, the belt deformation and its modal content should not be a priori decided, but rather incorporated in the transient study.

2.2. *Simulation of tyre shear force generation*

Shear force transient models, in contrast to the modal-oriented ones, focus on the accurate representation of the phenomena within the contact interface. Most of them are based on the brush or spoke theory [16], an extension of the Winkler bedding contact theory, whereby the dynamic contact behaviour of the tread is simulated by a number of viscoelastic elements. The structural deformation of the belt is taken into consideration only in respect to the effect it may have on the tread elements behaviour. A comprehensive account of such models can be found in [2].

Although brush models can offer a more realistic representation of the transient contact phenomena and can incorporate advanced friction models, the absence of a full tyre structure, or the simplifications in its deformation representation as introduced in [17], do not allow for the vertical load distribution to be accurately calculated. In many cases, the vertical load distribution is assumed to be an analytical function of the position along the contact, with the parabola being the favourable choice for simple analysis [2]. In an effort to improve accuracy, simplified physical contact models are used to capture the changes in the size of the contact and the associated vertical distribution, as shown in [18].

Some shear-force models incorporate a realistic carcass deformation pattern, as is the bending deformation of the discretized model presented in [19] and the semi-

analytical one in [20]. However, lack of inclusion of the dynamics of the whole tyre structure, limits the applicability of such approaches. The detached nature of the contact prevents the study of the interaction between carcass dynamics and contact force generation.

2.3. *Combined modal and shear force generation simulation*

It is clear that models with focus on vibration and shear force generation alike incorporate certain assumptions that impair their ability to simulate tyre behaviour under severely transient inputs. A substantial effort to overcome such limitations by combining a discretized model of the whole tyre structure with a detailed tread foundation model has lead to the generation of a family of tyre models described in [21]. The fine discretization which is essential for accurately capturing the contact phenomena and subsequently calculating the shear forces imposes a high computational load. These models are a popular choice for ride/comfort studies [22], given that the essential, severe, computational force and time can be provided.

2.4. *Tyre modal behaviour: Correlation between experimental and simulation results*

Having discussed the main modelling trends and their strengths/weaknesses, the focus is directed now towards the requirements for successful modelling of the interaction between modal behaviour and shear-force generation.

Given that any belt deformation must be composed by the superposition of a certain number of modes and their corresponding mode shapes, the actual number of contributing modes cannot be determined beforehand. Stick-slip friction, common in tyre-road interaction [18, 23], as well as other non-linearities, theoretically impose a rather broad-band excitation. In practice, such a wide frequency range is not present in the actual carcass response, due to energy dissipation reasons, but this cannot the only basis upon which a frequency cut-off limit is decided for a tyre model aiming to simulate modal/shear-force interactions.

An additional difficulty in determining what is an appropriate bandwidth for a tyre model follows from the inherent limitations of experimental modal tests. Due to practical difficulties associated with measurement methods [24] and the underlying damping mechanism, tyre modes cannot be identified above a rather low frequency limit. As a result, broad frequency range tyre modal behaviour above this limit cannot be strictly associated with a certain modelling approach. The case where the experimental frequency limit lies below the maximum value of the required frequency range can be interestingly studied with a number of different belt modelling approaches.

Numerous studies, [6, 25–27] verify that, within a given frequency range, excellent correlation is demonstrated between experimental results and the in-plane modal behaviour predicted by the analytical ring model. Beyond a frequency level, tyre modal behaviour is better represented by a thin plate under tension, as shown in [28]. As discussed in detail in [24], within the low frequency range, tyre modal behaviour is associated with pretension and circularity effects. As the frequency increases, bending stiffness becomes a more significant contributor.

In the following sections, a thorough comparative study is carried out to ascertain how accurately different modelling approaches capture the modal behavior of the tyre structure within a broad frequency range and the discretization effect is analyzed. The study also investigates the influence of internal air pressure and comments on the applicability of modal reduction techniques depending on the

model in use. This investigation follows from the recognition that modal reduction is an effective way to reduce computation time, as discussed in [4, 13, 14].

3. The ring model

3.1. *Equations of motion and eigen-analysis*

A typical ring model comprises three main elements :

- A thin circumferential bending beam representing the tyre belt.
- A radial and tangential stiffness foundation representing the tyre sidewall.
- A pretension condition representing the inflation of the tyre.

Thin ring vibration theory is analytically presented in [29, 30], while [31] represents the most comprehensive study on the vibrations of the ring and cylinder structures.

The two complete equations of motion read:

$$\frac{D}{R^4}(u_r^{''''} - u_\theta^{'''}) + \frac{K}{R^2}(u_r + u_\theta^{'}) + \frac{N}{R}(2u_\theta^{'} - u_r^{''}) + k_r u_r + bd\rho\ddot{u}_r = q_r + \frac{N}{R} \tag{1a}$$

$$\frac{D}{R^4}(u_r^{'''} - u_\theta^{''}) - \frac{K}{R^2}(u_r^{'} + u_\theta^{''}) - \frac{N}{R}(2u_r^{'} + u_\theta^{''}) + k_\theta u_\theta + bd\rho\ddot{u}_\theta = q_\theta \tag{1b}$$

where:

$u_r(\theta)$	radial deformation
$u_\theta(\theta)$	tangential deformation
b	width of the ring cross section
d	height of the ring cross section
ρ	ring material density
R	ring radius
$D = E\ b\ d^3/12$	bending stiffness of the ring
$K = E\ b\ d$	membrane stiffness of the ring
P_0	inflation pressure
$N = P_0\ b$	inflation tension force (circ. length normalized)
k_r	radial stiffness of the sidewall foundation (circ. length normalized)
k_θ	tangential stiffness of the sidewall foundation (circ. length normalized)
$q_r(\theta)$	radial external force excitation (circ. length normalized)
$q_\theta(\theta)$	tangential external force excitation (circ. length normalized)
$(')$	differentiation in respect to angle
$(\dot{})$	differentiation in respect to time

The ring model natural frequencies are calculated as follows:

- Deformation functions are written in modal form. As ring axissymmetry imposes harmonic mode shape functions, the deformations can be expressed as:

$$u_r = R(\theta)e^{i\omega_n t} \qquad u_\theta = \Theta(\theta)e^{i\omega_n t} \tag{2}$$

where:

Table 1. Ring model properties[a]

Property	E	ρ	P_0	R	b	d	k_r	k_θ
units	$kgr/(mm\ sec)$	kgr/mm^3	$kgr/(mm\ sec^2)$	mm	mm	mm	$kgr/(mm\ sec^2)$	$kgr/(mm\ sec^2)$
Value	10.4×10^6	8.1×10^{-6}	220	300	152	3.1	1.929×10^3	648.7

[a] after [3]

$R(\theta) = A\cos\big(n(\theta-\varphi)\big)$, $\Theta(\theta) = B\sin\big(n(\theta-\varphi)\big)$	mode shape functions
ω_n	natural frequency
A, B	mode shape amplitudes
n	modal number
φ	arbitrary angle which depends on the excitation orientation

- Zero external excitation is assumed and the equations are re-written in a matrix form:

$$\begin{bmatrix} \rho\ b\ d\ \omega_n^2 + C_1 & C_2 \\ C_3 & \rho\ b\ d\ \omega_n^2 + C_4 \end{bmatrix} \times \begin{bmatrix} A \\ B \end{bmatrix} = \begin{bmatrix} 0 \\ 0 \end{bmatrix} \tag{3}$$

where:

$$C_1 = -(\tfrac{D}{R^4}n^4 + \tfrac{N}{R}n^2 + \tfrac{K}{R^2} + k_r)$$

$$C_2 = C_3 = -\tfrac{D}{R^4}n^3 - (\tfrac{K}{R^2} + 2\tfrac{N}{R})n$$

$$C_4 = -(\tfrac{D}{R^4} + \tfrac{K}{R^2} + \tfrac{N}{R})n^2 - k_\theta$$

- The characteristic equation of the coefficient matrix of eqn. 3:

$$(\rho\ b\ d)^2\ \omega_n^4 + \rho\ b\ d\ (C_1 + C_2)\ \omega_n^2 + C_1\ C_2 - C_3\ C_4 = 0 \tag{4}$$

The solution of the trinomial (4) for every mode number $n \geq 0$ offers two frequency values and two modes. Substituting the calculated natural frequency in (3) we acquire the ratio between radial and tangential deformation for every ring point, the so called mode shape of the mode. The one of the two modes is associated with primal radial deformation while the other one with tangential deformation. For typical tyre-correlating ring properties, the radial modes correspond to lower frequency values than the tangential ones. Such properties are included in table 1, after[3]. The first five ($n = 0$ to 4) radial and tangential mode shapes are presented in fig. 1.

3.2. *Simplifications*

A simplified version of the equations of motion is presented by Kung in [32]. The non linear terms $\frac{P_0}{R}2u_\theta'$ and $-\frac{P_0}{R}(2u_r' - u_\theta'')$ are omitted from the eqn. 1a and eqn. 1b respectively.

Another common simplification is the inextensibility assumption, as firstly presented in [5], according to which radial and tangential deformation are coupled

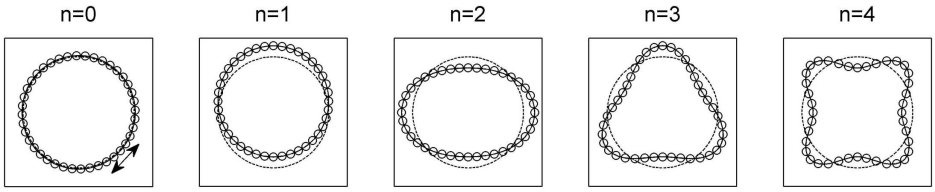

(a) radial mode shapes

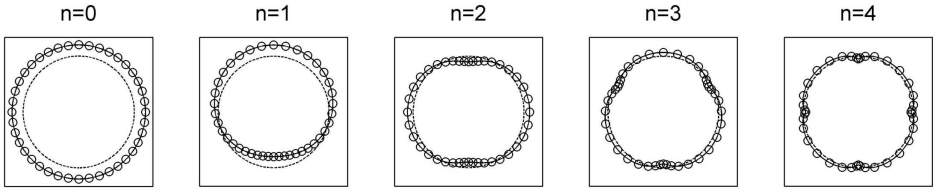

(b) tangential mode shapes

Figure 1. Ring model mode shapes

through the relationship:

$$u_{\theta}^{'} = -u_r \tag{5}$$

Natural frequencies under this assumption are given by the equation:

$$\omega_n^2 = \frac{n^2(1-n^2)^2 D}{R^4 \rho\ b\ d\ (1+n^2)} + \frac{P_0\ b\ n^2\ (1-n^2)}{R\ \rho\ b\ d} + \frac{k_r\ n^2 + k_\theta}{\rho\ b\ d\ (1+n^2)} \tag{6}$$

3.3. *Zero and rigid modes*

The modal number of every $n \geq 1$ mode dictates the complete periods of characteristic deformation which can be identified in the mode shape; the n*th* mode of radial deformation, for example, is associated with a mode shape in which n complete periods of radial deformation can be observed.

This convention is not valid for the zero modes, where a spatially constant deformation (zero period) is associated with the supplementary deformation direction to the one that the mode name refers to. In particular the radial zero mode is identified by a constant tangential deformation (torsional movement of the ring around the wheel), while the tangential zero mode is identified as a constant radial deformation of the whole ring. It is also evident from eqn. 3 that zero modes predict zero value for the deformation their name refers to, since all non diagonal values of the coefficient matrix (C_2 and C_3) become zero for $n = 0$.

Substituting $n = 0$ in the equation 4 yields :

$$(4) \xrightarrow{n=0} \begin{cases} \omega_{n=0}^{rad} = \sqrt{\frac{k_\theta}{\rho\ b\ d}} \\ \\ \omega_{n=0}^{tang} = \sqrt{\frac{K+K_r\ R^2}{R^2\ \rho\ b\ d}} \end{cases} \tag{7}$$

The radial zero mode frequency is only affected by the tangential sidewall stiffness, while the tangential zero mode frequency is a function of the ring membrane stiffness and the radial sidewall stiffness.

At this point, it is worth noting the difference between eqn. 1 and those presented in [9–11, 15, 26], in terms of the incorporation of inflation pressure. In [9–11, 15, 26], a term proportional to the inflation pressure is multiplied directly by the radial

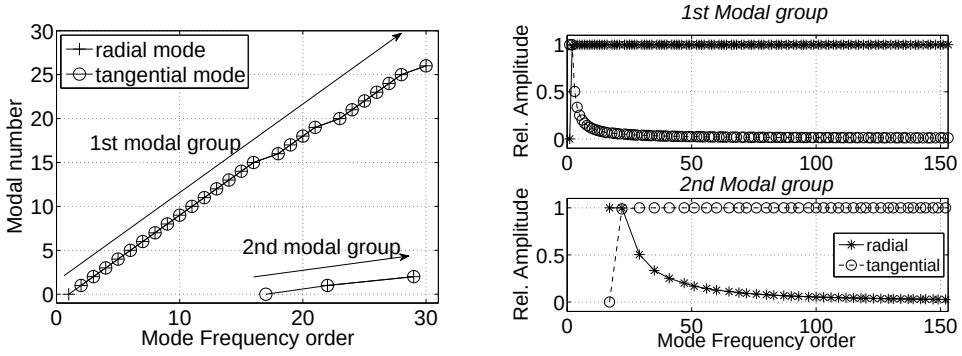

(a) Radial and tangential ring modal groups.

(b) Relative amplitude of radial /tangential deformation for each mode shape.

Figure 2. Analytical ring model modal behaviour.

and tangential displacements in the corresponding radial and tangential equations of motion. Although this is derived from a correct mathematical procedure, the provided equations predict that the frequencies of both radial and tangential zero modes depend also on inflation pressure. This was thought not to be applicable to our case since the radial $n = 0$ mode should provide the rotational rigid mode of the ring when omitting the sidewall foundation. As the prediction of the ring rigid modes by the equations of motion is vital for the non linear sidewall case, the approach presented herein was chosen.

The ring can be mathematically treated as a two-dimensional simplification of the cylindrical shell, thus the comprehensive and systematic presentation of the shell equations of motion by Leissa in [31] is regarded as highly valuable. Interestingly, a large number of shell theories cannot predict the in-plane rigid motion, associated with the unsuspended n=0 and n=1 modes. Although the pretension existence makes the above shortcoming even more intense, experimental results [31] prove the insignificance of the pretension effect on the related modes. In conclusion, the pretension effect should be incorporated in the ring model under careful consideration of the shortcoming of the followed approach, regarding the critical n=0 and n=1 modes.

3.4. *Ring model predicted modal behaviour*

In order to present the ring modal behaviour, we plot the first 30 modes and their modal number, according to their natural frequency order (fig. 2(a)). Their separation into two groups of modes (radial-tangential) is clear and results from the existence of two natural frequencies for each modal number. In an attempt to generalize this feature of modal behaviour we define a modal group as a sequence of modes, corresponding to a strictly increasing or decreasing order of modal number. The increase of modal number naturally corresponds to an increase in the frequency. However, another modal group (the tangential one in the examined case) may unfold within a common frequency window, with its modal numbers not corresponding to the modal numbers of the first group within the window. As can be seen in fig. 2(a) the two modal groups scatter into each other.

The relative radial / tangential amplitude of deformation corresponding to each mode is presented in fig. 2(b) for a broad modal range of 150 modes in total. The amplitudes are normalized, by dividing with the maximum amplitude (radial or tangential) of each shape, so that the maximum amplitude equals unity. Apart from the pure tangential deformation corresponding to the zero radial mode and

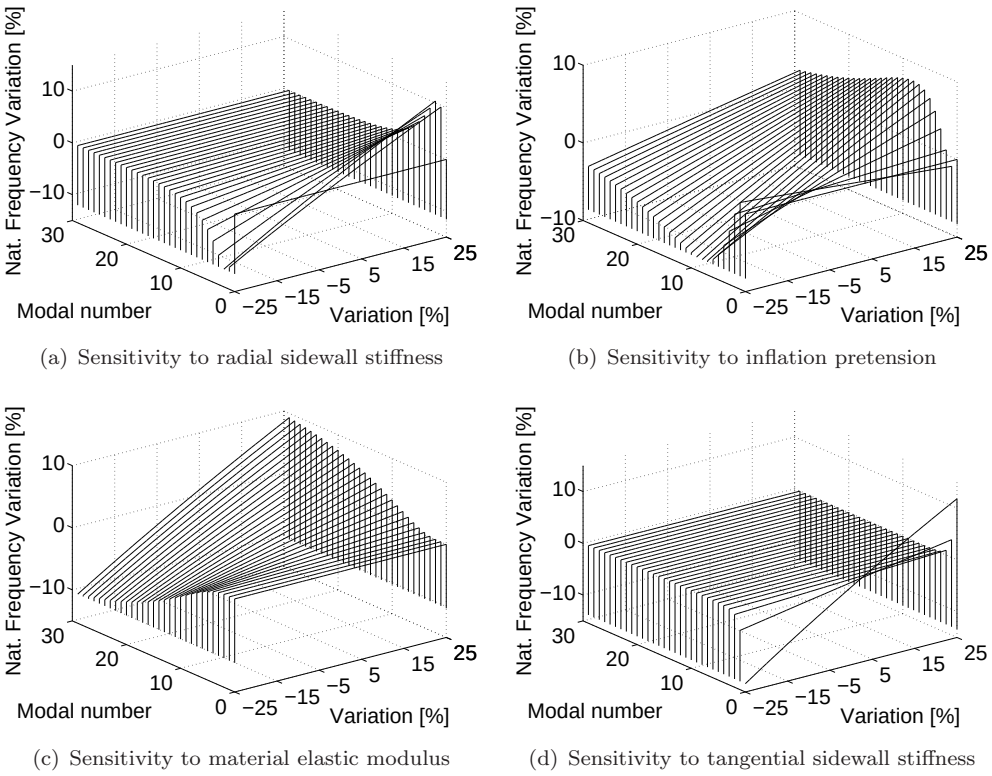

(a) Sensitivity to radial sidewall stiffness

(b) Sensitivity to inflation pretension

(c) Sensitivity to material elastic modulus

(d) Sensitivity to tangential sidewall stiffness

Figure 3. Ring model radial modes sensitivity to ring material elastic modulus, inflation pretension, radial and tangential sidewall stiffness

the almost equal radial/tangential deformation observed in the $n = 1$ mode, the rest of the radial modes (1st modal group) show a common deformation trend. The tangential component of the $n > 1$ mode shapes decreases, approaching asymptotically zero for very high modal numbers. Tangential modes (2nd modal group) develop in an analogous manner. The tangential zero mode exhibits purely radial deformation (breathing), while the $n = 1$ mode is characterized by equal participation of both radial and tangential deformations. All other modes show an asymptotic reduction in the participation of radial deformation in the mode shape pattern.

3.5. *Modal sensitivity analysis*

The dependence of zero modes on certain tyre properties is evident in eqn. 1, the qualitative effect, though, cannot be easily identified. In order to examine the effect of each property on the natural frequencies, a sensitivity analysis is performed. Imposing percentage variations to the basic properties proposed in table 1, we can identify which of the properties play a major role in the characterization of the modal behavior of the ring.

A $\pm 25\%$ variation has been imposed on the ring material elastic modulus ,inflation pressure and radial and tangential sidewall stiffness. The resulting natural frequency variation of each of the 30 first modes,presented in fig. 3, is used as a sensitivity criterion for the dependence on the ring parameters.

Starting with the radial modes, it is observed that the influence of radial sidewall stiffness is significant in the very low frequency range, maximizes for $n = 2$, and can be practically neglected for $n > 10$ (fig. 3(a)). Similarly, inflation pretension affects the natural frequency values in the low to medium frequency range. Its effect

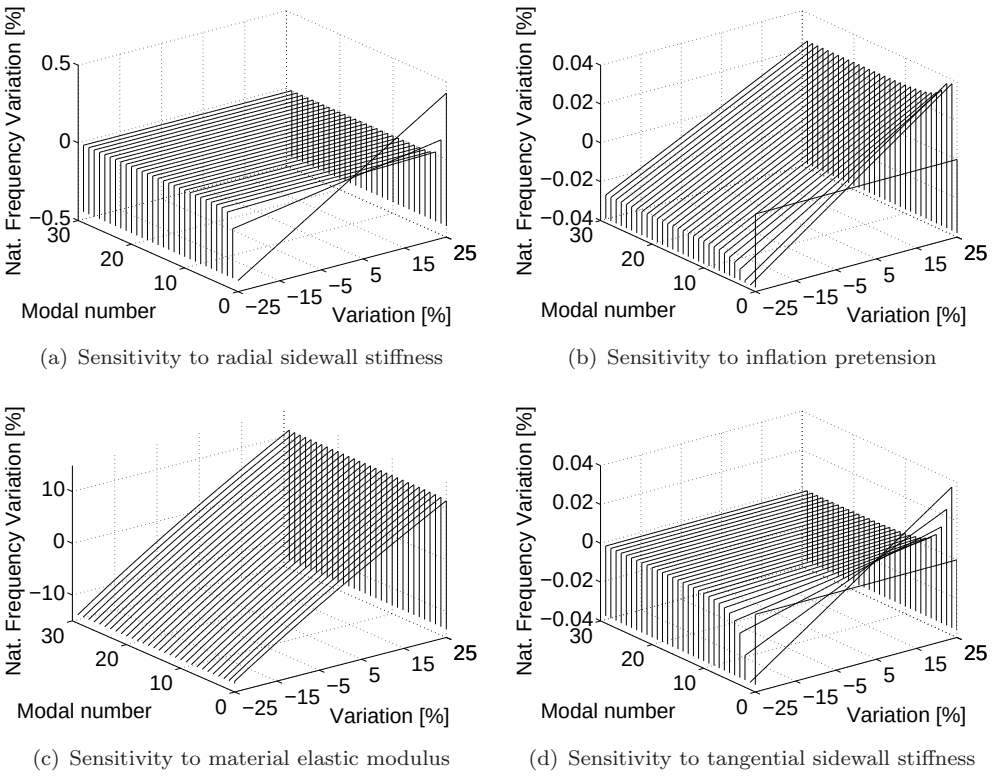

(a) Sensitivity to radial sidewall stiffness

(b) Sensitivity to inflation pretension

(c) Sensitivity to material elastic modulus

(d) Sensitivity to tangential sidewall stiffness

Figure 4. Ring model tangential modes sensitivity to ring material elastic modulus, inflation pretension, radial and tangential sidewall stiffness

maximizes around the $n = 10$ mode while it deteriorates for higher modal numbers (fig. 3(b)). The elastic modulus of the material has an increasing influence with modal number, being the primary contributor of frequency variation for $n > 20$, but can be neglected for $n < 10$ (fig. 3(c)). These three ring model properties constitute the main frequency regulation mechanism, each one of them affecting a certain range of modes. The dependence of radial modes is completed with the study of the influence of tangential sidewall stiffness, which is strong in the first two modes (the mode shapes of which exhibit significant tangential deformation) but can be neglected for higher modal numbers.

The above analysis is in agreement with the experimental tyre model identification presented in [24]. According to this study, pretension (expressed here by the sidewall and the inflation effect) is the dominant contributor when it comes to low frequency modal behaviour, while bending stiffness (property proportional to the material elastic modulus) dominates higher frequencies. For this reason, the ring model better represents tyre modal behaviour in the low-to-medium frequency range, while a bending plate model shows better correlation with experimental results in the higher frequency range, at least up to the frequency measurement limit.

As the frequency range of the tangential modal group usually exceeds the experimentally observable range (with the possible exception of the breathing mode), the analysis of the second modal group cannot be experimentally verified. Numerical results are presented in fig. 4, although these refer to a frequency range where the actual tyre modal behaviour cannot be assumed as two-dimensional. Varying the elastic modulus of the material equally influences the frequencies of all modes (fig. 4(c)). Changing inflation pretension has an impact on all modes of so small magnitude that the effect can be neglected (fig. 4(b)). The effect of the sidewall

stiffness is also negligible (fig. 4(a) and fig. 4(d)), with the possible exception of the effect of radial sidewall on the very first tangential modes ($n \leq 5$).

Thus far, the main aspects of the modal behavior predicted by the ring model have been presented, covering a broad frequency range, which exceeds the limit of experimental observations. It is emphasized that, at higher frequencies, the response of the tyre structure becomes three-dimensional and the validity of an in-plane analysis gradually deteriorates. Although this study is restricted to in-plane dynamics, the future requirement of accurate prediction of the contact deformation, calls for the inclusion in the study of such a broad modal range.

4. Discretized tyre modelling approach

Tyre modal behaviour can be simulated by discretized models, consisting of a variety of different types of elements. A finite element tyre model was developed in [33], resulting from revolution of an axisymmetric thin shell. This model was used for modal behaviour prediction in [32, 34]. A non-linear sidewall element is described in [35], while a model focused on the simulation of the contact is presented in [36]. A detailed discussion on discretized modelling approaches can be found in [37, 38].

Models aiming to simulate combined modal/contact behaviour tend to be more complicated than the ones focusing on pure modal prediction, consisting of a combination of different types of elements, which characterize different sections of the tyre structure. This combined simulation approach is found in the commercially available FTire model [21], or the advanced contact representation described in [39] and [38]. The requirement for the accurate capture of the contact behaviour and friction-related phenomena, such as stick-slip, has led to the separate treatment of the contact using finer discretization levels than those required for modal representation ([18]).

Pacejka in [2], following the analysis initially presented in [40], divides shear force generation models according to the included type of carcass compliance as:

- Models that exclude the bending of the belt, or string models
- Models that include the bending stiffness of the belt, or beam models

Conforming to the classification suggested above, the extent to which discretized models accurately predict tyre modal behaviour will be investigated using models based on two different types of finite elements:

(1) A one-dimensional linear truss element for the case where the bending stiffness of the belt is ignored.
(2) An extensible linear beam element for the case where bending stiffness is considered.

The inertia and stiffness matrix formulation for both elements is presented in Appendix A. A number of such elements substitutes the analytical ring in the representation of the belt. The elements are rotated and coupled to each other so that the whole structure will represent the circular tyre shape, although composed by straight elements. The distributed sidewall elastic foundation transforms into an equal discretized one, attached to every node. As none of the linear finite elements can represent the effect of inflation pretension on modal behaviour, the effect of its exclusion will be investigated and possible compensating techniques will be proposed.

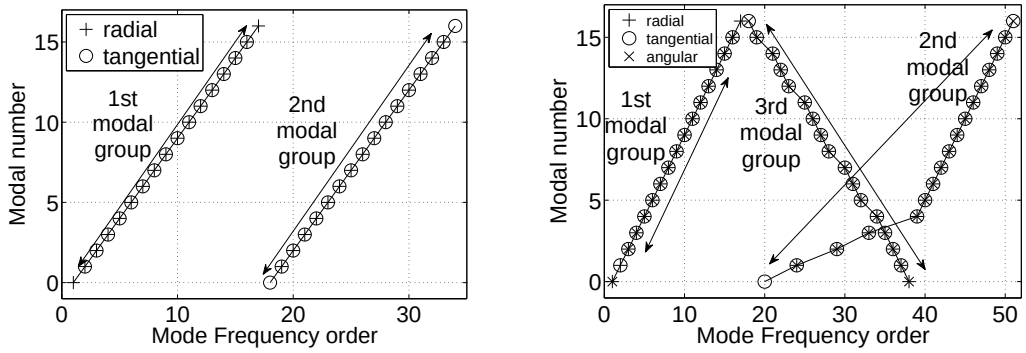

(a) Truss model modal groups.

(b) Beam model modal groups

Figure 5. Modal groups development prediction of the discretized models (m=32).

4.1. *General modal behaviour of the discretized models*

The number of predicted modes in any discretized structure equals the number of degrees of freedom and transition from a space to a modal representation can be seen as a coordinate transformation. The double axis symmetry of the structure imposes the duplicity of all modes with modal number $n \geq 1$ and the singular existence of the $n = 0$ modes, in a direct space to modal transformation. The two mode shapes corresponding to the same mode present a relative rotation angle of $\frac{pi}{2n}$ with respect to each other. The total number of zero modes equals the number of degrees of freedom per node, a. In order to preserve the double axis symmetry of the models an even number, m, of elements is required, which results in an odd total number of the $n \geq 1$ modes. As a result, the modes with modal number from $n = 1$ to $n = \frac{m}{2} - 1$ appear as double while the $n = 0$ and $n = \frac{m}{2}$ modes appear as single.

The notion of modal groups, presented in section 3.4 for the analytical ring model, is now applied to the description of the modal behaviour of discretized models. Considering a discretized model, a modal groups can be identified in its modal representation, where:

$$m\ elements \rightarrow a \times m\ DOFs \rightarrow a \times m\ modes \rightarrow a \times modal\ groups \rightarrow$$

$$a \times \begin{cases} 1 \times \ n = 0\ mode \\ 2 \times \{n = 1\ ...\ n = \frac{m}{2} - 1\}\ modes \\ 1 \times \ n = \frac{m}{2}\ mode \end{cases} \tag{8}$$

Prior to examining the natural frequencies predicted by each of the discretized models, some general trends are examined. The relation between frequency order and modal number for the truss and beam models are presented in fig. 5(a) and fig. 5(b), respectively, for the same number of elements ($m = 32$).

4.2. *Truss model modal behaviour*

The truss model predicts two distinct modal groups. The normalized contributions of radial and tangential deformations in the corresponding mode shapes is shown in fig. 6(a). The first modal group exhibits a primarily radial deformation, in agreement with the predictions of the analytical ring model. Similarly, the second modal group is characterized by a predominantly tangential deformation, as is the second modal group of the analytical ring model. In both groups, the supplementary defor-

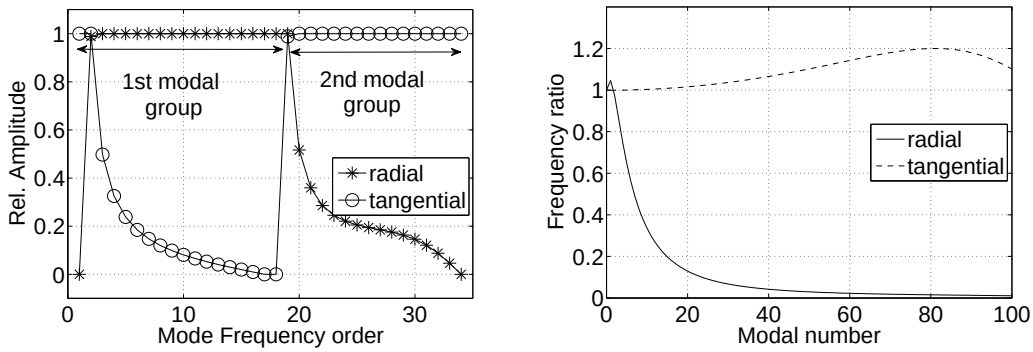

(a) Relative radial/tangential deformation of the truss model predicted mode shapes (m=32).

(b) Complete (m=200) modal range frequencies ratios of the truss and the ring models' modes, corresponding to the same modal number and modal group.

Figure 6. The truss model predicted modal behaviour.

mation decreases with the modal number, as in the analytical ring case. However, as the $2nd$ modal group always develops after the end of the first one, the total frequency order of the modes depends on the number of elements. Subsequently, this observation raises questions with regards to the application of modal reduction techniques to the truss model, in case the procedure is based only on the frequency order of the selected modes.

Although, shape-wise, the modes predicted by the truss model show good agreement with those predicted by the ring modes (as can be concluded by the comparison of fig. 2(b) and fig. 6(a)), frequency-wise this is not the case. The latter is illustrated in 6(b), where the frequency ratio between truss and ring modes is plotted as a function of the corresponding modal number, for the whole frequency range predicted by a $m = 200$ elements truss model. The radial modes predicted by the truss model correspond to much lower natural frequencies than those generated by the ring model, with this discrepancy intensified as the modal number increases. The natural frequencies corresponding to tangential modes show much better correlation; however, at relatively high modal numbers, the discretized model tends to overestimate the tangential natural frequencies to an extend depending on the total available modal range.

The tendency of the truss model to separate radial from tangential modes and the predicted natural frequencies deviation from the ring ones, even for low modal numbers - low frequency range , appear as major shortcomings, which prevent the model from providing accurate modal representation. These shortcomings result from the combined effect of three distinct factors, namely the lack of bending stiffness, lack of inflation pretension and the discretization effect.

The behaviour of the truss model can be further explained by considering the ring model sensitivity analysis presented in fig. 3 and fig. 4. At low frequencies, sidewall stiffness regulates the frequency content of the first few radial modes of the ring. Accordingly, the agreement in the frequencies associated with the first radial modes of the truss and ring models can be attributed to the influence of the sidewall foundation which is common in the two models. As the modal number increases, the frequency correlation between truss and ring radial modes deteriorates, as a result of the lack of inflation pretension effect in the truss model. This can be justified by observing fig. 3(b) and is also discussed in [24]. Finally, the lack of bending stiffness in the truss model is associated with the very large frequency discrepancies observed at high modal numbers. Considering that bending stiffness is directly proportional to the elastic modulus, this conclusion is supported by fig.

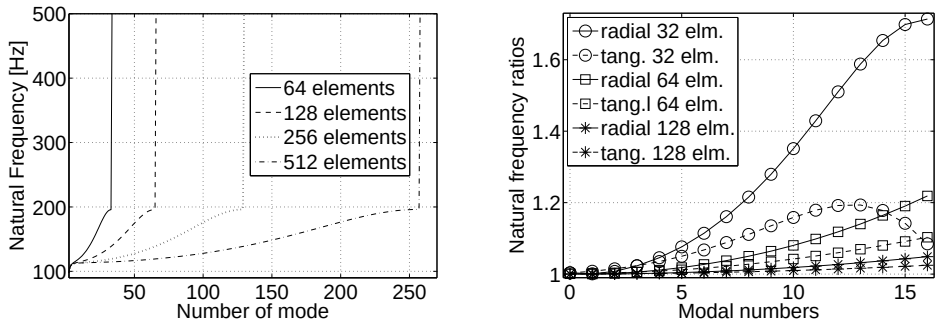

(a) Complete range truss model predicted natural frequencies for various number of elements.

(b) Discretization effect on the truss model predicted radial and tangential modes, as a function of the total number of elements.

Figure 7. The discretization effect on the truss model predicted modal behaviour.

3(c), as well as the analysis presented in [24].

Focusing on the tangential modes, the elastic modulus of the material is primarily responsible for the tangential stiffness of both the truss and ring models. The axial stress mechanism can be equally prescribed by the truss element (Appendix A) and the ring equations of motion (eqn. 1),in contrast to the bending behaviour, which cannot be prescribed by both of them. In addition, as the inflation pretension has a negligible effect on the frequency of the tangential modes of the ring (fig. 4(b)), its absence does not affect the correlation of the tangential frequencies. In total, the tangential mode frequencies show good correlation for a wide range of modal numbers. For a number of relatively high mode numbers, the agreement between ring and truss models seems to deteriorate, with the truss model predicting higher frequencies compared to the ring model. This appears to be related to the discretization effect, as the modal number above which frequency discrepancies start to become significant is a function of the total number of modes predicted by the truss model.

4.3. *Truss model discretization effect*

The general effect of discretization on the truss model is presented in fig. 7. As expected, an increase in the number of truss elements results in a direct increase in the number of available modes and the maximum frequency observed. This is clearly depicted in figure 7(a). Interestingly, the same graph reveals that the frequency corresponding to a specific mode decreases as the discretization becomes finer (more elements are implemented in the model), with this difference becoming enormous above a mode associated with the total modal range of the model.

The effect of discretization is investigated further using a 512 element model as a basis for comparison. Three different discretized models with 32, 64 and 128 elements, respectively, are compared with the reference model in terms of the frequencies associated with the first 17 radial and tangential modes. The results are presented in fig. 7(b) in the form of frequency ratios where the frequency predicted by the 512 element model for a specific mode is used as the denominator.

Clearly, the frequencies predicted by models with fewer elements deviate quickly towards higher values. In addition, the deviation is more pronounced for the radial modes. The latter is associated with the fact that as the number of elements increases, the number of modes (m) that correspond to the frequency range up to the breathing mode increases, since the two groups do not scatter. At the same time, though, the frequency range of the $1st$ modal group remains constant, from the

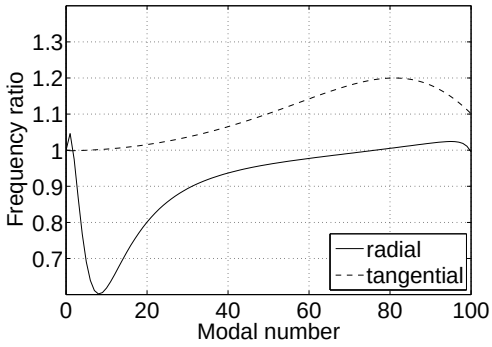

Figure 8. Complete range (m=200) natural frequencies ratios of the radial/tangential frequencies of the beam model to the corresponding analytical ring predicted ones.

torsional mode frequency to the breathing one, both frequencies being the least affected by the total number of elements (the discretization effect is minimal in the beginning of the modal groups). As a result, the frequency associated with a certain mode decreases for higher number of elements.

This behaviour is not so provocative for the tangential group case as the upper limit of its frequency range is not constant, but directly associated with the total number of elements (fig. 7(a)). The discretization effect should be taken into consideration when a subset of modes is selected in order to describe the tyres behaviour using a modal reduction technique.

4.4. *Beam model modal behaviour*

Prior to examining the modal behaviour of the beam model, it should be clarified that, apart from the inflation pretension effect and the artificially imposed discretization one, no other differences exist between the physical vibration mechanism described by the analytical ring and the beam-based models. It should be noted, though, that a third modal group is predicted by the discretized beam model, as shown in fig. 5(b). This modal group is related to the spatial derivative of the radial degree of freedom with respect to the tyre circumference, i.e. it is related to the existence of the bending angle as a distinct degree of freedom in the beam model.

A major difference between the two discretized models, which should be taken into consideration in modal reduction procedures, is that the frequency order of the first two beam predicted modal groups is constant and the scattering positions of the one into each other is not associated with the total number of elements. The latter was the case in the truss model, where the modal groups developed sequentially. A selection of a certain number of modes according to their frequency order is composed by the same modes in the beam case, independently from the total number of elements. In contrast, the possible incorporation of tangential modes into this group in the truss case, heavily depends on the total number of elements.

The relative amplitudes of radial/tangential deformation of the modes composing the first two modal groups are similar to the ones predicted by the analytical ring. The total modal range natural frequency ratios implemented for comparison between the discretized beam ($m = 200$) and ring models are presented in fig. 8,for both the radial and the tangential modal groups. A large frequency deviation is observed at lower mode numbers for the radial modes and is attributed to the lack of inflation pretension in the discretized beam model,as this deviation maximizes in the modal range primarily affected by the inflation pressure variations (fig.

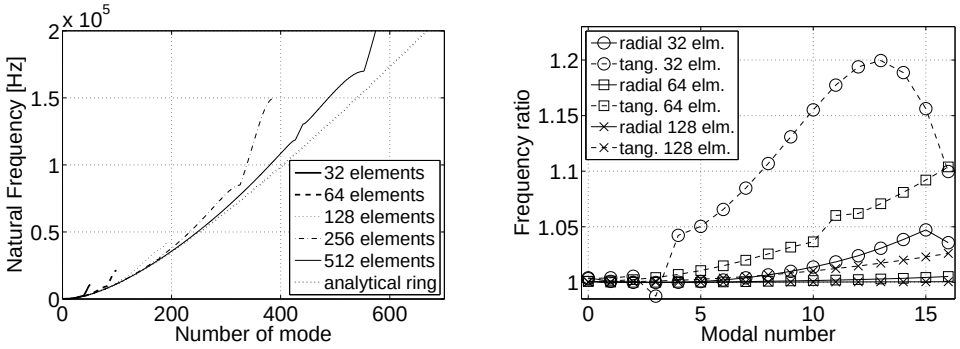

(a) Complete range beam model predicted natural frequencies for various number of elements.

(b) Discretization effect on the beam model predicted radial and tangential modes, as a function of the total number of elements.

Figure 9. Discretization effect on beam model predicted natural frequencies.

3(b)). The frequencies predicted by the two models show better correlation as the modal number increases, since the effect of inflation pretension diminishes and the stiffening effect due to discretization comes into play.

In general, the inclusion of bending stiffness in the modelling approach has significantly improved the correlation between discretized and analytical ring models, as a direct comparison of fig. 6(b) and fig. 8 reveals. The minimal effect of inflation pretension on the tangential modes is, as in the case of the truss model, responsible for the good frequency correlation characterizing the tangential groups, up to a limit imposed by the discretization effect.

4.5. *Beam model discretization effect*

The effect of discretization on the beam model is presented in fig. 9(a), where the whole frequency range predicted by models with different number of elements is plotted in direct comparison to the frequencies obtained by the analytical ring model, assuming zero pretension. At higher mode numbers, an artificial stiffening of the modes predicted by the discretized beam models is evident. The mode number above which this stiffening effect is intense, is closely related to the total number of available modes. In particular, as the number of elements increases, the deviation starts at higher mode numbers, a common behaviour with the truss model.

The frequency response of the discretized beam models is compared with that of the analytical ring, without pretension, through their frequency ratios. The frequency ratios for the first 17 modes are presented in fig. 9(b) for both the radial and tangential groups and for discretized models with a different number of elements. The effect in general is not as intense as in the truss case, as the comparison of fig. 9(b) with fig. 7(b) reveals. Discretization affects the tangential modes more than the radial ones, in contrast to the truss model. In this case the frequency range of the tangential group extends from the breathing mode (the frequency of which is not affected by the number of elements) to a frequency clearly associated with the number of elements. The much broader frequency range of this group, results in its association with higher discretization effect.

4.6. *Superposition of the inflation effect on beam modal behaviour*

Following the analysis presented in the previous section, it appears that the main shortcoming of the discretized beam model is the lack of accuracy in the low-to-medium frequency range of its radial response,given that the number of examined

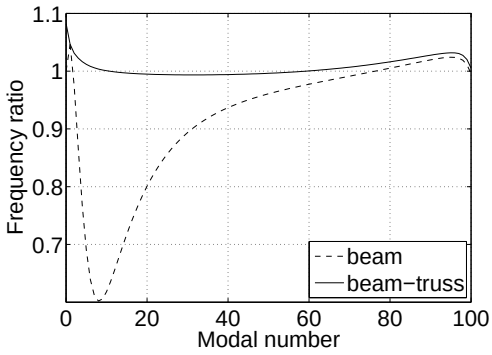

Figure 10. Radial frequencies ratios of the beam and combined beam-string models to the corresponding analytical ring predicted ones.

modes is significantly lower than the available range so that the discretization effect can be neglected. This has been attributed to the omission of the pretension effect due to inflation pressure.

The membrane-type response of the tyre is experimentally noticed in [24], within the low frequency modal response of the tyre. The inflation-associated mechanism has been utilized in many modelling concepts (string/mebrane models). A study of the tyre belt as a continuous, inextensible string was initially proposed by Pacejka in [41] and is presented in detail in [2], while a discretized two-dimensional (membrane) modelling approach is described in [42].

Herein, the physical mechanism of inflation pretension will be simulated by the implementation of a series of inextensible string elements along the circumference of the tyre. The string elements are parallel to the beam ones and they share they same nodes wit them. They offer additional to the beam, inflation dependent stiffness in the vertical to the element axis, in-plane direction. The concept is further explained in Appendix B1. The inertia behaviour of the enchanted model remains unchanged.

The development of modal groups and the relative contributions of radial/tangential deformations in each mode remain unchanged compared to the simple beam model. The ratios of the radial frequencies of the combined beam-string model to the ring predicted ones are presented in fig. 10, in comparison to the simple beam model ratios, previously presented in fig. 8. No significant change develops in the tangential frequencies, so they are omitted from the presentation. A significant improvement in the radial response's correlation with the ring one is evident, in the whole frequency range and especially in the range mainly affected by the inflation pretension.

5. The effect of sidewall non-linearity on tyre modal behaviour

The effect of inflation pressure is not limited to the resulting circumferential pretension of the belt presented in the previous section. Acting on the tyre sidewall, air pressure directly influences its stiffness in the radial direction. In turn, provided the inflation pressure, the radial stiffness of the sidewall depends on its current radial displacement. The importance of the inclusion of sidewall non linearity in a vehicle dynamics oriented tyre model was recognized by Böhm in [6], while a finite element formulation combining a string-based sidewall and a beam-based belt can be found in [35]. A complete modal study using a tyre model incorporating a string/beam based sidewall is presented in [43].

A typical tyre sidewall is a relatively thin structure composed of several cord

layers of high tensile strength. This morphology justifies the choice of a membrane or string (when focusing on a cross-section of the tyre circumference) in order to represent the displacement-dependent radial stiffness of a tyre. This dependency results from the non-linear development of the string force as well as the orientation of this force with respect to the radial direction. The latter is related to string geometry and also varies with radial displacement. A brief presentation of the string-based sidewall foundation implemented herein is provided in Appendix B2.

In summary, inflation pressure increase affects radial sidewall stiffness in 2 ways:

- A variation in inflation pressure results in a change of the inflated radius of the tyre, imposing a new equilibrium geometry for the sidewall string and resulting in a new string force. The non-linear relationship (see Appendix B2) between the force and the radial distance from the belt to the wheel results in a different radial stiffness for every equilibrium shape.
- The string force is proportional to the inflation pressure, so a stiffness variation is induced by a change in air pressure, even without considering any changes in string geometry.

5.1. *String effect implementation*

A string-based, non-linear sidewall can be implemented in both the analytical ring model and the discretized beam model with additional circumferential string elements. The steps described below are followed for the study of the interaction between inflation pressure and sidewall stiffness and the resulting influence on tyre modal behaviour.

(1) The normalized (to circumferential length) radial force generated by a string-based sidewall foundation is calculated for a range of radial displacements and inflation pressures. The resulting set of force vs displacement data for every inflation pressure value is fitted by a polynomial function (fig. 11).
(2) For each inflation pressure, the effect of inflation pretension on the belt alone is incorporated as dictated by the analytical equations of the ring (eqn. 1), or through the circumferential string elements implemented in the enhanced discretized beam model. In both cases, the inflation-induced change in the belt radius is neglected, only for this part of the calculation.
(3) A dynamic simulation of the inflation procedure is performed in order to determine the equilibrium point of the whole tyre structure for the chosen inflation pressure. Both tyre models are equipped with the string-based sidewall and their belt equations are updated as described in step 2. The tyre models are initially assumed deflated. Inflation pressure is applied as a step-excitation and the tyre models are left to reach equilibrium. The equilibrium point is registered in terms of the corresponding radial deflection, as is the force generated by the sidewall.
(4) The equilibrium point found in the previous step is located on the polynomial curve fitted in step 1. The slope of the curve at equilibrium is analytically calculated by differentiating the polynomial curve at that point. The linear radial stiffness at the given equilibrium point is equal to the slope of the curve.
(5) The process is repeated with different pressures in order to obtain a number of equilibrium points and the corresponding linear sidewall stiffness for a range of inflation pressures.
(6) The effect of inflation pressure variation on the predicted tyre modal behaviour will be associated with the belt stiffening incorporated in the second step and the sidewall stiffness variation calculated in step 4.

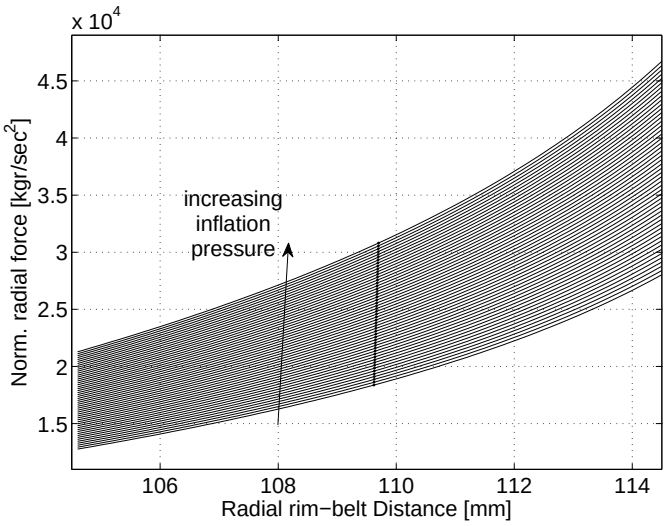

Figure 11. The radial sidewall force (length normalized) as a non linear function of inflation pressure and radial wheel-belt distance. The equilibrium inflation distance for every pressure value (±25% of the initial value) is marked.

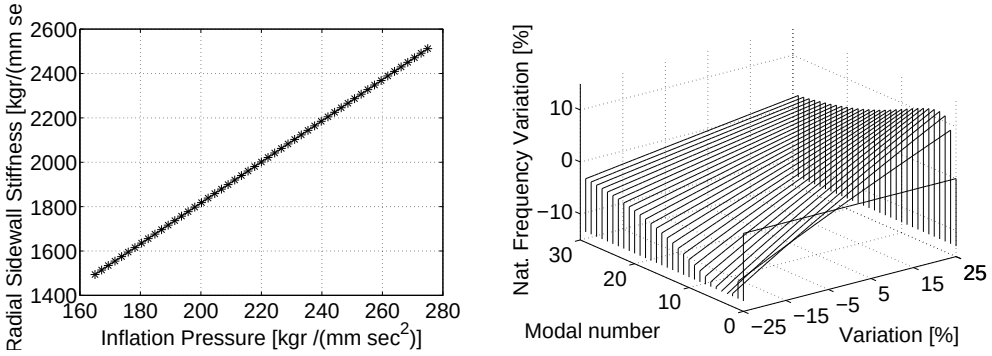

(a) Radial sidewall stiffness (length normalized) as a function of inflation pressure, as it resulted from the linearization procedure.

(b) Revised calculation of inflation variation effect on ring model natural frequencies, as a combined effect on sidewall and ring belt stiffness.

Figure 12. The effect of inflation pressure variation on radial natural frequencies, including the non linear sidewall effect.

5.2. *Numerical example and results*

As a case study, the procedure described above is applied on the analytical ring model only, assuming a typical $15in$ ($381mm$) wheel diameter. The nominal radial belt-to-wheel distance is $109.5mm$, which is also regarded as the initial value for dynamic inflation. Assuming a reasonable string arc length of $122mm$, the calculated radial sidewall stiffness is found to agree closely with the one given in table 1, for the same inflation pressure. A ±25% variation in the initial inflation pressure value of table 1 is assumed, in accordance to the sensitivity analysis presented in fig. 3.

Each curve in fig. 11 corresponds to a different inflation pressure value. The equilibrium position resulting from the dynamic solution is marked on all curves. It is evident that inflation pressure has a significant effect on the radial force, however the radial deflection at different equilibrium points hardly changes with pressure. This is a result of circumferential belt stiffness which prevents the tyre structure from expanding considerably. Considering the proportionality between the string force and inflation pressure (see Appendix B2), the significant increase

in the level of radial force and the radial stiffness alike is primarily related to the increase in inflation pressure and secondarily to the geometric variation of the string elements.

The radial sidewall stiffness as a function of inflation pressure, is presented in fig. 12(a). The significant stiffness variation, almost proportional to inflation pressure, influences considerably the tyres modal behaviour, a contribution neglected in the results presented in fig. 3(b). The sensitivity of the frequencies of radial modes on changes in inflation pressure is illustrated in 12(b), including the effect of a pressure dependent sidewall stiffness. The results could be explained as a combination of the uncoupled sensitivities to inflation pressure and radial sidewall stiffness, described previously in fig. 3(b) and fig. 3(a).

6. Conclusions

An in-depth study of the potential, in terms of accurately predicting tyre modal behaviour, of a number of frequently used tyre modelling approaches has been carried out. The ultimate aim, of which a preliminary part is the present study, is to choose an appropriate approach for the satisfactory tyre modal simulation in a broad frequency range, associated with the processes taking place at the tyre contact patch during severe handling manoeuvres.

Macroscopically, vehicle handling analysis is concerned with low frequency dynamic phenomena. Tyre models aimed at handling studies tend to neglect high frequency structural responses. Most such models assume an a-priori known contact condition and would only consider the lower frequency vibratory modes of the tyre. In studies aiming to dynamically generate the contact conditions it is important to be aware of the ability of the tyre model in hand to accurately predict the deformation pattern of the belt when in contact with the ground. This ability is not merely a function of the highest frequency that can be achieved by any given tyre model. The accurate reproduction of various mode shapes is also of great importance and would directly influence the generated contact shape and pressure distribution, as the contact deformation is reproduced through the superposition of the available mode shapes.

In the present study, the analytical ring model has been used as a benchmark due to its experimental validation, albeit up to a rather low frequency limit. The modal response of the ring model has been compared with that of two discretized models, namely a truss-based and a beam-based model. The lack of bending stiffness from the truss model resulted in poor simulation of the radial response throughout the frequency range, except for very low frequencies. The discretized beam model performed much better than the truss model with its only weakness being the inability to cater for the effect of inflation pressure on the pretension of the tyre belt. This was corrected by adding circumferential string elements, in parallel configuration to the beam ones, resulting in an enhanced model which achieved almost perfect agreement with the predictions of the ring model.

The predictions of both discretized models were subject to a discretization-induced stiffening (increase in the corresponding frequencies) of the modes, as the modal number approached the modal limit imposed by the total number of the available degrees of freedom. This finding should be taken into consideration when deciding on the number of elements incorporated in a discretized tyre model and is also relevant when applying a modal reduction/expansion technique for solving a discretized tyre model in a computationally efficient manner.

Both the analytical ring and the enhanced discretized beam models were further improved by the addition of a non-linear sidewall represented by an inextensible

string. This enhancement permitted the prediction of the effect of inflation pressure on the radial stiffness of the sidewall and showed that the overall contribution of inflation pressure on modal response is much more significant than that attributed to the stiffening of the belt alone.

The analysis presented herein offers a solid understanding of the inherent characteristics of various modelling approaches and provides an idea of the features required in a tyre model, if it is to achieve accuracy within a wide frequency range. It is thought that this knowledge is particularly important when deriving in-plane vibratory models capable of generating a dynamically changing contact pressure distribution. Finally, the findings may form a source of valuable advice when it comes to making decisions during the set-up and parameter identification stages for existing tyre models, such as the FTire. In particular, the number of elements included in the model, or the number of modes used for the identification of its parameters may be chosen in relation to the requirements of the task in hand and the results provided in the present paper.

References

[1] A. Noor, K. Kim, and J. Tanner, *Analysis of aircraft tires via semianalytic finite elements*, Finite Elements in Analysis and Design 6(3) (1990), pp. 217–233.
[2] H. Pacejka *Tyre and Vehicle Dynamics*, Butterworth-Heinemann, 2006.
[3] P. Zegelaar, *Modal Analysis of Tire In-Plane Vibration*, SAE Paper (1997), pp. 149–172.
[4] I. Lopez et al., *Modelling vibrations on deformed rolling tyres a modal approach*, Journal of Sound and Vibration 307(3-5) (2007), pp. 481–494.
[5] J. Tielking, *SAE Paper 6504925, Midyear Meeting, Chicago, IL*, Plane vibration characteristics of a pneumatic tire model (1965).
[6] F. Böhm, *Mechanik des Gürtelreifens*, Archive of Applied Mechanics (Ingenieur Archiv) 35(2) (1966), pp. 82–101.
[7] W. Soedel and M. Prasad, *Calculation of natural frequencies and modes of tires in road contact by utilizing Eigenvalues of the axisymmetric non-contacting tire*, Journal of Sound and Vibration 70(4) (1980), pp. 573–584.
[8] S. Huang and W. Soedel, *Effects of coriolis acceleration on the free and forced in-plane vibrations of rotating rings on elastic foundation*, Journal of Sound and Vibration 115(2) (1987), pp. 253–274.
[9] S. Huang and W. Soedel, *Response of rotating rings to harmonic and periodic loading and comparison with the inverted problem*, Journal of Sound and Vibration 118 (1987), pp. 253–70.
[10] S. Huang and B. Hsu, *An approach to the dynamic analysis of rotating tire-wheel-suspension units*, Journal of Sound and Vibration 156(3) (1992), pp. 505–519.
[11] S. Huang, *Vibration of rolling tyres in ground contact*, International Journal of Vehicle Design 13(1) (1992), pp. 78–95.
[12] K. Johnson *Contact Mechanics*, Cambridge University Press, 1987.
[13] E. Rustighi and S. Elliott, *Stochastic road excitation and control feasibility in a 2D linear tyre model*, Journal of Sound and Vibration 300(3-5) (2007), pp. 490–501.
[14] F. Wullens and W. Kropp, *A Three-Dimensional Contact Model for Tyre/Road Interaction in Rolling Conditions*, Acta Acustica united with Acustica 90(4) (2004), pp. 702–711.
[15] Y.H. Wijnant and A. De Boer, *A new approach to model tyre/road contact*, Proc. of ISMA (Leuven, Belgium) (2006), pp. 4453–4462.
[16] H. Pacejka and R. Sharp, *Shear Force Development by Pneumatic Tyres in Steady State Conditions: A Review of Modelling Aspects*, Vehicle System Dynamics 20(3) (1991), pp. 121–175.
[17] P. Zegelaar, S. Gong, and H. Pacejka, *Tyre Models for the Study of In-Plane Dynamics*, Vehicle System Dynamics 23 (1994), pp. 578–590.
[18] G. Mavros, H. Rahnejat, and P. King, *Transient analysis of tyre friction generation using a brush model with interconnected viscoelastic bristles*, Proceedings of the Institution of Mechanical Engineers, Part K: Journal of Multi-body Dynamics 219(3) (2005), pp. 275–283.
[19] G. Mastinu and M. Fainello, *Study of the Pneumatic Tyre Behaviour on Dry and Rigid Road by Finite Element Method*, Vehicle System Dynamics 21(1) (1992), pp. 143–165.
[20] G. Mastinu et al., *A Semi-Analytical Tyre Model for Steady-and Transient-State Simulations*, Vehicle System Dynamics 27 (1996), pp. 2–21.
[21] M. Gipser, *FTire: a physically based application-oriented tyre model for use with detailed MBS and finite-element suspension models*, Vehicle System Dynamics 43(1) (2005), pp. 76–91.
[22] A. Riepl, W. Reinalter, and G. Fruhmann, *Rough road simulation with tire model RMOD-K and FTire*, Vehicle System Dynamics 41(SUPPL) (2004), pp. 734 – 743.
[23] M. Kuwajima, M. Koishi, and J. Sugimura, *Contact Analysis of Tire Tread Rubber on Flat Surface with Microscopic Roughness*, Tire Science and Technology 34(4) (2006), pp. 237–255.
[24] J. Perisse, J. Clairet, and J. Hamet, *Modal testing of a smooth tire in low and medium frequency-estimation of structural parameters*, SPIE proceedings series (2000), pp. 960–967.
[25] G. Potts et al., *Tire vibrations*, Tire Science and Technology 5(1) (1977), pp. 202–225.

[26] J. Perisse and J. Hamet, *A comparison of the 2d ring and 3d orthotropic plate for modelling of radial tire vibrations*, Proceedings of the Internoise 2000 Conference, Nice, France (2000).
[27] Z. Geng, A. Popov, and D. Cole, *Measurement, identification and modelling of damping in pneumatic tyres*, International Journal of Mechanical Sciences 49(10) (2007), pp. 1077–1094.
[28] W. Kropp *Ein Modell zur Beschreibung des Rollgeräusches eines unprofilierten Gürtelreifens auf rauher Strassenoberfläche*, Ph.D. diss., Düsseldorf, 1992.
[29] W. Weaver, S. Timoshenko, and D. Young *Vibration Problems in Engineering*, Wiley-Interscience, 1990.
[30] W. Soedel *Vibrations of Shells and Plates*, CRC Press, 2004.
[31] A. Leissa *Vibration of Shells (NASA SP-288)*, Washington, DC: US Government Printing Office (republished for the Acoustical Sociey of America through the American Institute of Physics), 1973(1993).
[32] L. Kung, W. Soedel, and T. Yang, *Free vibration of a pneumatic tire-wheel unit using a ring on an elastic foundation and a finite element model*, Journal of Sound and Vibration 107(2) (1986), pp. 181–194.
[33] C. Hunckler *The dynamic behaviour of an automobile tyre*, Ph.D. diss., Purdue University, 1979.
[34] Y. Chang, T. Yang, and W. Soedel, *Dynamic analysis of a radial tire by finite elements and modal expansion*, Journal of Sound and Vibration 96(1) (1984), pp. 1–11.
[35] C. Mousseau and G. Hulbert, *The dynamic response of spindle forces produced by a tire impacting large obstacles in a plane*, Journal of Sound and Vibration 195(5) (1996), pp. 775–796.
[36] J. Pelc, *Towards realistic simulation of deformations and stresses in pneumatic tyres*, Applied Mathematical Modelling 31(3) (2007), pp. 530–540.
[37] L. Faria et al., *Tire Modeling by Finite Elements*, Tire Science and Technology 20(1) (1992), pp. 33–56.
[38] K. Danielson, A. Noor, and J. Green, *Computational strategies for tire modeling and analysis*, Computers and Structures 61(4) (1996), pp. 673–693.
[39] J. Oden and E. Pires, *Algorithms and numerical results for finite element approximations of contact problems with non-classical friction laws*, Computers and Structures 19(1) (1984), pp. 137–147.
[40] F. Frank *Theorie des Reifenschräglaufs*, Ph.D. diss., Braunschweig, 1965.
[41] H. Pacejka, *Analysis of the Dynamic Response of a Rolling String-Type Tire Model to Lateral Wheel-Plane Vibrations*, Vehicle System Dynamics 1(1) (1972), pp. 37–66.
[42] S. Saigal et al., *Free vibrations of a tire as a toroidal membrane*, Journal of Sound and Vibration 107(1) (1986), pp. 71–82.
[43] R. Pinnington, *Radial force transmission to the hub from an unloaded stationary tyre*, Journal of Sound and Vibration 253(5) (2002), pp. 961–983.
[44] M. Bhatti *Fundamental finite element analysis and applications: with mathematica and matlab computations*, Hoboken, New Jersey: John Wiley & Sons, 2005.
[45] T.R. Zienkiewicz O.C. *The FInite Element Method For Solid and Structural Mechanics*, Butterworth-Heinemann, 2005.

Appendix A. Discretized finite elements formulation

The total number of degrees of freedom of a belt model composed by m elements (and m modes) will be $a \times m$, where a is the number of global degrees of freedom assigned to each node.

The local-to-global transformation for the truss model results in twice as many degrees of freedom, according to:

$$a_{local} : axial\ deformation \rightarrow \begin{cases} a^1_{global} : horizontal\ deformation \\ a^2_{global} : vertical\ deformation \end{cases}$$

The stiffness and inertia matrices for a representative truss element in the global frame of reference are expressed as:

$$K_{truss} = \frac{EA}{l} \begin{bmatrix} 1 & 0 & -1 & 0 \\ 0 & 0 & 0 & 0 \\ -1 & 0 & 1 & 0 \\ 0 & 0 & 0 & 0 \end{bmatrix} \tag{A1}$$

$$M_{truss} = \frac{\rho A l}{6} \begin{bmatrix} 2 & 0 & 1 & 0 \\ 0 & 2 & 0 & 1 \\ 1 & 0 & 2 & 0 \\ 0 & 1 & 0 & 2 \end{bmatrix} \tag{A2}$$

where:

E	material elastic modulus
A	cross-section area
l	finite element length
ρ	material density

The two matrices are presented in their complete (4×4) form, including the normal to the length of the element degrees of freedom, which come into play after the local-to-global transformation. This does not affect the stiffness matrix, as the strain energy depends on the deformation along the length of the element, but is important for the inertia matrix, since motion along both axes is characterized by inertia force ([44]).

The number of degrees of freedom per node for the beam based model is not affected by the global transformation:

$$\left.\begin{matrix} a^1_{local} : axial\ deformation \\ a^2_{local} : normal\ deformation \end{matrix}\right\} \rightarrow \begin{cases} a^1_{global} : horizontal\ deformation \\ a^2_{global} : vertical\ deformation \end{cases} \\ a^3_{local} : angular\ deformation \rightarrow a^3_{global} : angular\ deformation \tag{A3}$$

The stiffness and inertia matrices for the beam element are :

$$K_{beam} = \begin{bmatrix} \frac{EA}{l} & 0 & 0 & -\frac{EA}{l} & 0 & 0 \\ 0 & \frac{12EI}{l^3} & \frac{6EI}{l^2} & 0 & -\frac{12EI}{l^3} & \frac{6EI}{l^2} \\ 0 & \frac{6EI}{l^2} & \frac{4EI}{l} & 0 & -\frac{6EI}{l^2} & \frac{2EI}{l} \\ -\frac{EA}{l} & 0 & 0 & \frac{EA}{l} & 0 & 0 \\ 0 & -\frac{12EI}{l^3} & -\frac{6EI}{l^2} & 0 & \frac{12EI}{l^3} & -\frac{6EI}{l^2} \\ 0 & \frac{6EI}{l^2} & \frac{2EI}{l} & 0 & -\frac{6EI}{l^2} & \frac{4EI}{l} \end{bmatrix} \tag{A4}$$

$$M_{beam} = \frac{\rho A l}{420} \begin{bmatrix} 140 & 0 & 0 & 70 & 0 & 0 \\ 0 & 156 & 22l & 0 & 54 & -13l \\ 0 & 22l & 4l^2 & 0 & 13l & -3l^2 \\ 70 & 0 & 0 & 0 & 140 & 0 \\ 0 & 54 & 13l & 0 & 156 & -22l \\ 0 & -13l & -3l^2 & 0 & -22l & 4l^2 \end{bmatrix} \tag{A5}$$

The nomenclature follows the one of eqn. A1 and eqn. A2, while I is the second moment of inertia of the cross-section.

Appendix B. String equations

B.1. *String circumferential element*

The differential equation governing transverse vibrations of an inextensible rectilinear string under tension force is:

$$T\frac{\partial^2 U_y}{\partial x^2} = \rho A \frac{\partial^2 U_y}{\partial t^2} \tag{B1}$$

where:

T	the tension force
U_y	the normal to the string length deformation
$\frac{\partial}{\partial x}$	partial differentiation with respect to the position along the string
ρ	string material density
A	the cross-section area
$\frac{\partial}{\partial t}$	partial differentiation with respect to time

In order to express the string behaviour described by eqn. B1 in a discretized way, we assume rectilinear string elements of the same length with the beam ones, sharing the same nodes with them. The two degrees of freedom of each string element coincide with the normal degrees of freedom of the beam.

Although equation B1 refers an initially straight string, for the calculation of the tension force only, we assume that the string is arc-shaped, with a radius equal to that of the ring (see fig. 1(a)). Thus, the tension force caused by the inflation may be calculated according to:

$$T = P_0 \cdot R \cdot b \tag{B2}$$

P_0	the inflation pressure
R	the belt radius
b	the belt width

For the expression of the string element behaviour in a stiffness-equivalent way, a linear interpolation method [45] is assumed. The process is similar to the one followed in the case of the stiffness matrix of the truss element, although in this case the interpolated deformation (U_y) lies in the normal to the tension direction. The resulting, stiffness-equivalent, matrix is:

$$K_{string} = \frac{T}{l}\begin{bmatrix} 1 & -1 \\ -1 & 1 \end{bmatrix} \rightarrow K_{string} = \frac{P_0 R b}{l}\begin{bmatrix} 1 & -1 \\ -1 & 1 \end{bmatrix} \tag{B3}$$

where l is the element length.

The updated stiffness matrix of the beam element so as to include the inflation-dependent contribution of the string element, reads:

$$K_{beam-string} = \begin{bmatrix} \frac{EA}{l} & 0 & 0 & -\frac{EA}{l} & 0 & 0 \\ 0 & \frac{12EI}{l^3} + \frac{P_0 R b}{l} & \frac{6EI}{l^2} & 0 & -\frac{12EI}{l^3} - \frac{P_0 R b}{l} & \frac{6EI}{l^2} \\ 0 & \frac{6EI}{l^2} & \frac{4EI}{l} & 0 & -\frac{6EI}{l^2} & \frac{2EI}{l} \\ -\frac{EA}{l} & 0 & 0 & \frac{EA}{l} & 0 & 0 \\ 0 & -\frac{12EI}{l^3} - \frac{P_0 R b}{l} & -\frac{6EI}{l^2} & 0 & \frac{12EI}{l^3} + \frac{P_0 R b}{l} & -\frac{6EI}{l^2} \\ 0 & \frac{6EI}{l^2} & \frac{2EI}{l} & 0 & -\frac{6EI}{l^2} & \frac{4EI}{l} \end{bmatrix} \tag{B4}$$

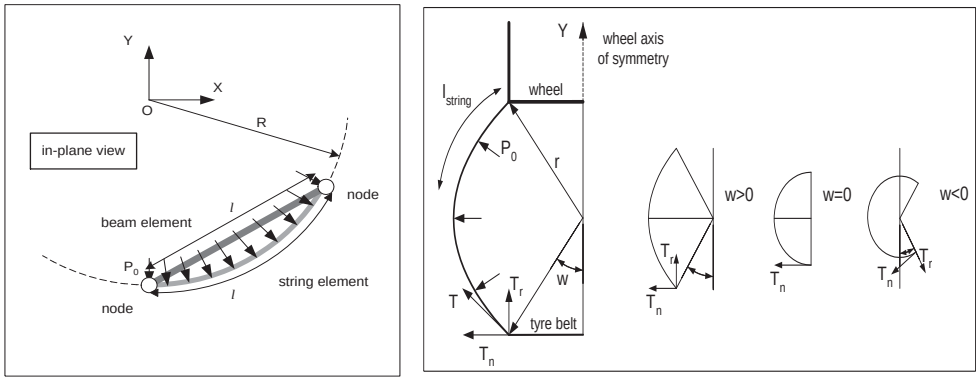

(a) The combined beam - string element of the belt.

(b) The string elements of the radial sidewall foundation (T: the tension force, tangential to the string, T_r: the radial component, T_n: the lateral component).

Figure B1. The two applications of the string physical mechanism.

B.2. *String sidewall foundation*

The geometry of the sidewall string is presented in fig. 1(b), as is the resulting force direction for different deformation cases. Based on this geometry, the following equation is derived:

$$\left.\begin{array}{l} \frac{\pi-2w}{l_{string}} = \frac{1}{r} \\ \cos w = \frac{L}{2\cdot r} \end{array}\right\} \quad \rightarrow \quad L(\pi - 2w) = 2l_{string} \cdot \cos w \tag{B5}$$

where:

r	the sidewall radius
L	radial distance between the belt and the wheel
w	angle prescribed in fig. 1(b)
l_{string}	length of the string

Assuming that the total width of the sidewall string element is equal to the circumferential length of the belt, the radial sidewall force per length of the tyres circumference can be expressed as :

$$T^{norm} = P_0 r \xrightarrow{(B5)} T_r^{norm} = P_0 l_{string} \frac{sin\omega}{\pi - 2\omega} \tag{B6}$$

We should notice that during the inflation dynamic simulation, described in section 5, the non linearity of the string mechanism, formulated in B5, necessitates an iteration procedure for the calculation of the sidewall force, in each time step. For a given radial deformation L the iteration algorithm solves the eqn. B5, determines the angle ω and calculates the resulting radial force.